![HOKKAIDO UNIVERSITY]

Title	Characterization of mouse mediastinal fat-associated lymphoid clusters
Author(s)	Elewa, Yaser Hosny Ali; Ichii, Osamu; Otsuka, Saori; Hashimoto, Yoshiharu; Kon, Yasuhiro
Citation	Cell and Tissue Research, 357(3), 731-741 https://doi.org/10.1007/s00441-014-1889-6
Issue Date	2014-09
Doc URL	http://hdl.handle.net/2115/59758
Rights	The final publication is available at link.springer.com
Type	article (author version)
Additional Information	There are other files related to this item in HUSCAP. Check the above URL.
File Information	CellTissueRes v.357 p.731.pdf

Instructions for use

1 **Characterization of mouse mediastinal fat-associated lymphoid clusters**

2 Yaser Hosny Ali Elewa[1,2], Osamu Ichii[2], Saori Otsuka[2], Yoshiharu Hashimoto[3], Yasuhiro Kon[2,]*

3 [1]Department of Histology and Cytology, Faculty of Veterinary Medicine, Zagazig

4 University, Zagazig 44519, Egypt

5 [2]Laboratory of Anatomy, Department of Biomedical Sciences, Graduate School of

6 Veterinary Medicine, Hokkaido University, Sapporo 060-0818, Japan

7 [3]Office for International Accreditation of Veterinary Education, Obihiro University of

8 Agriculture and Veterinary Medicine, Obihiro 080-8555, Japan

9

10 ***Corresponding author**: Yasuhiro Kon, DVM, PhD, Laboratory of Anatomy, Department of

11 Biomedical Sciences, Graduate School of Veterinary Medicine, Hokkaido University, Kita 18, Nishi

12 9, Kita-ku, Sapporo 060-0818, Japan. y-kon@vetmed.hokudai.ac.jp

13

14

15

16   **Abstract**

17   The association between adipose tissue and immunity has been established, and fat-associated

18   lymphoid clusters (FALCs) are considered a source of immune cells. We discovered lymphoid

19   clusters (LCs) in mouse mediastinal fat tissues (MFTs). In three mice strains, including Th1-biased

20   C57BL/6N (B6), Th2-biased DBA/2Cr (DBA), and autoimmune-prone MRL/MpJ (MRL), LCs

21   without a fibrous capsule and germinal center were observed in white-colored MFTs extending from

22   the diaphragm to the heart. The number and size of the LCs were larger in 12-month-old mice than

23   in 3-month-old mice in all of the examined strains. Moreover, B6 had an especially large number of

24   LCs compared with DBA and MRL. The immune cells in the LCs consisted of mainly T-cells and

25   some B-cells. The majority of T-cells were CD4+ helper T (Th) cells, rather than CD8+ cytotoxic

26   T-cells, and there was no obvious immune cell population difference among three mouse strains.

27   Furthermore, high endothelial venules and lymphatic vessels were well developed in the LCs of B6

28   mice than other strains. Interestingly, few CD133+ hematopoietic progenitor cells and few

29   c-Kit+/CD127+ natural helper cells were detected in the LCs. BrdU+ proliferating cells were

30   abundantly detected in the LCs of B6 mice compared to other strains and tended to increase with

31   ages. This is the first report of LCs in mouse MFTs and we suggest that the size and number of LCs

32   are affected by the mouse genetic background. We termed the LCs mediastinal fat-associated

33   lymphoid clusters (MFALCs). These clusters may be considered niches for Th cell production.

34   **Key words:** mediastinal, adipose tissue, lymphoid cluster

35

Introduction

Adipose tissue is a specialized connective tissue distributed throughout the body. It acts as a cushion and stores lipids as energy sources. Furthermore, adipose tissue has been recognized as a major endocrine organ, producing hormones and adipokines such as leptin, estrogen, resistin, and tumor necrosis factor alpha (Kershaw and Flier 2004). Recently, lymphoid clusters (LCs) were observed in the adipose tissue of human and mouse mesentery; they were termed fat-associated lymphoid clusters (FALCs) (Moro et al. 2010). FALCs are in direct contact with adipocytes, lack fibrous capsules, and contain T-cells, B-cells, macrophages, and dendritic cells and are also found around the kidney and genital organs (Koyasu and Moro 2011). They are structurally similar to the milky spot in the omentum, which is considered a gateway of cells between the circulation and the peritoneal cavity (Cranshaw and Leak 1990). However, unlike the milky spot, T-cell and B-cell zones or germinal center structures are not observed in FALCs (Moro et al. 2010). Results from retinoic acid receptor-related orphan receptor gamma (RORγ)-deficient mice and alymphoplasia (aly/aly) mice suggested that the differentiation pathway of FALCs is distinct from that of lymph nodes or Peyer's patches (Nishikawa et al. 2003).

There are 2 major subsets of helper T (Th) cells, Th1 and Th2 cells, differentiated by the pattern of cytokine production (Fiorentino et al. 1989). Th1 cytokines include interleukin 2 (IL-2), IL-12, and interferon gamma (IFN-γ), which are associated with the activation of cellular immunity. Th2

54 cytokines include IL-10, IL-4, IL-5, and IL-6, which are associated with humoral immunity. In

55 addition to these Th cells, Th17 cells producing IL-17 have been identified, and these cells are

56 considered critical for the development of autoimmune disease (Bettelli et al. 2007).

57

58   The cooperation of innate and adaptive immune responses is critical for protective immunity

59 against infection (Zygmunt and Veldhoen 2011). B-cells and T-cells are the major types of cells

60 involved in the adaptive or acquired immune system. In addition to two prototypic innate

61 lymphocyte populations, namely classical natural killer (NK) and lymphoid tissue inducer (LTi) cells,

62 recent studies have identified Th2-type innate lymphocytes, such as Nh cells (Moro et al. 2010 and

63 Koyasu and Moro 2011).

64   Interestingly, such novel Th2-type innate lymphocyte, natural helper (Nh) cells express c-Kit,

65 Sca-1, interleukin-2 receptor (IL-2R), interleukin-7 receptor (IL-7R), and IL-33R were found in the

66 FALC. Nh cells in the FALC produce Th2 cytokines, including IL-5 and IL-13, and play important

67 roles in innate and anti-helminthes immunity (Moro et al. 2010). The IL-7R consists of two chains,

68 the IL-7R α-chain (IL-7Rα; also known as CD127) and the common cytokine-receptor γ-chain (γc;

69 also known as CD132) (Mazzucchelli and Durum, 2007). Recent studies revealed that CD127 is also

70 expressed by mouse natural killer (NK) lineage cells early during differentiation (Chiossone et al.

71 2009) as well as by the gut lamina propria CD56+CD3− NK cells (Takayama et al. 2010).

72   Autoimmune disease models such as the MRL/MpJ-lpr/lpr (MRL/*lpr*) mice develop

73   autoantibody production, lymphadenopathy, and glomerulonephritis associated with Th1 responses,

74   similar to human systemic lupus erythematosus. In contrast, abnormal Th2 skewing in MRL/*lpr*

75   altered the feature of nephritis from proliferative to membranous glomerulonephritis, with an altered

76   balance of Th1 (IFN-γ) and Th2 (IL-4) cytokine production (Shimizu et al. 2005). Shimizu et al.

77   reported that the imbalance of Th responses is associated with autoimmune phenotypes. Interestingly,

78   it has been reported that the genetic background of mice influences the Th responses. Briefly, mouse

79   strains favoring a Th1 response include C57BL/6, C57BL/10, and B10.D2/nSn, and those favoring a

80   Th2 response include DBA/2, BALB/c, BALB/cBy, BALB.B, and BALB.K (Linda et al. 2000;

81   Charles et al. 2000). These differences in Th responses are caused by differences in the genetic

82   background of the mice, and the susceptibility to several diseases, such as skin tumor, pneumonia,

83   and obesity, differs between C57BL/6 and DBA/2 (Gudmundsson et al. 1998; Butler et al. 2002).

84   In the present study, we found LCs associating with mediastinal fat tissues (MFTs) and termed

85   them mediastinal fat-associated lymphoid clusters (MFALCs). Furthermore, the size and lymphocyte

86   number of the MFALCs differed among the studied mouse strains: Th1-biased C57BL/6, Th2-biased

87   DBA/2, and autoimmune-prone MRL/MpJ. This is the first report of strain-specific differences in

88   MFALC structures, and we hypothesize that these differences are associated with the individual

89   characteristics of the immune responses in these strains.

90

91

92   **Materials and methods**

93   *Experimental animals*

94   C57BL/6N (B6), DBA/2Cr (DBA), and MRL/MpJ (MRL) mice were used in the present study.

95   Eight- to ten-week-old mice purchased from Japan SLC (Hamamatsu, Shizuoka, Japan) were

96   maintained with free access to specific pathogen-free food and water in our facility and were used at

97   3 and 12 months of age. In handling the experimental animals, the investigators adhered to the Guide

98   for the Care and Use of Laboratory Animals, Hokkaido University, Graduate School of Veterinary

99   Medicine (approved by the Association for Assessment and Accreditation of Laboratory Animal Care

100   International).

101

102   *Tissue preparation and microscopic observation*

103   After euthanasia by deep inhalation anesthesia, MFTs within the mediastinum extending from

104   the caval foramen of the diaphragm to the heart and the thymus were removed and fixed with 4%

105   paraformaldehyde (Fig. 1). After overnight fixation, specimens were washed in distilled water,

106   stained using the whole-mount hematoxylin method, and observed under a stereomicroscope after

107   penetration by glycerol. For histological examination, the removed MFTs were dehydrated in graded

108   alcohol and embedded in paraffin. Subsequently, 3-μm paraffin sections of MFT were deparaffinized,

109   rehydrated, stained with hematoxylin and eosin (HE), and observed by light microscopy.

Immunohistochemistry

111   Using the MFT sections, immunohistochemical analysis for B220, BrdU, CD3, CD4, CD8,

112   CD133, peripheral node addressin (PNAd), and lymphatic vessel endothelial hyaluronic acid

113   receptor 1 (LYVE-1) was performed to detect B-cells, pan T-cells, Th cells, cytotoxic T (Tc) cells,

114   hematopoietic progenitor cells (HPC), high endothelial venules (HEV), and lymphatic endothelial

115   cells, respectively. The immunohistochemical procedures were performed according to previous

116   reports (Elewa et al. 2010a).

117   The details of the antigen retrieval methods as well as the sources and dilutions of the

118   antibodies are listed in Table 1. For the detection of proliferating cells, 5-bromo-2-deoxyuridine

119   (BrdU) (Wako Pure Chemical Industries, Tokyo, Japan) was dissolved in PBS and injected

120   intraperitoneally into mice at 100 mg per kg of body weight. The MFTs were removed from the

121   animals 2 hr after BrdU injection. To detect BrdU-labeled cells, the MFT paraffin sections were

122   stained with rat anti-BrdU antibody (Table 1). The immunopositive reactions were developed in

123      $3,3'$-diaminobenzidine-H_2O_2 solution. The sections were counterstained with hematoxylin. Sections

124   of spleen were used as positive controls and stained by different antibodies simultaneously with the

125   MFTs. The sections for negative controls were stained with isotype control Ig at the same

126   concentration with the primary antibody or incubated in 0.01 M PBS without primary antibody (data

127   not shown).

128   *Immunofluorescence*

129   Immunofluorescence for c-Kit and CD127 was also performed to detect the Nh cells. The

130   deparaffinized sections were treated with 10 mM citrate buffer (pH 6.0) for 20 min at 105° C,

131   treated with normal donkey serum, and incubated at 4° C overnight with goat anti-c-Kit antibody

132   (1:100) and rabbit anti-CD127 antibody (1:1000) (Table 1). The sections were then incubated with

133   Alexa Fluor 488-labeled donkey anti-goat IgG and Alexa Fluor 546-labeled donkey anti-rabbit IgG

134   (1:500; Life Technologies) for 30 min, followed by Hoechst33342 (1:2000; Dojindo, Kumamoto,

135   Japan) for 3 min. The immunofluorescence signals were examined by confocal microscopy.

136

137   *Histoplanimetry*

138   Light micrographs of 5 whole-mount specimens as well as paraffin sections of the MFTs from

139   each strain were prepared for histoplanimetry. In the digital images of the sections, the areas of the

140   LCs were observed as dark regions in the MFTs. LCs and MFTs were measured using the ImageJ

141   software (ver. 1.32j, http://rsb.info.nih.gov/ij), and the LC-to-MFT ratio was calculated (as reported

142   in a previous study by Elewa et al., 2010b). Based on the immunohistochemical study, the numbers

143   of B220-, CD3-, CD4-, and CD8-positive cells in the LCs were counted in 3 different sections of the

144   MFTs from each mouse strain. In each section, the number of immunonegative cells was also

145   counted, and the percent of immunopositive cells among total cells was calculated as the positive

146 cell index for each cell population. The average of the indices for each cell population was

147 presented.

148

149 *Statistical analysis*

150   All numerical results were shown as the mean ± standard error (SE). The results of different

151 groups were compared using analysis of variance (ANOVA). We used the Tukey's post-hoc test for

152 multiple comparisons when a significant difference was observed by ANOVA ($p < 0.05$).

153

154

155

156

157

158

159

160

161

162

163

164

Results

LCs in mouse MFTs

The MFTs were observed as white-colored fat tissue in the mediastinum, extending from the

caval foramen of the diaphragm to the heart (Fig. 1). The localization of the MFTs was not

significantly different among the examined mice (data not shown). In the stereomicroscopic

observations of the whole-mount hematoxylin specimens, the examined MFTs from all mice showed

dark-stained regions that varied in shape and size (Fig. 2a–f), and these regions were confirmed as

LCs by subsequent histological examination (Fig. 3). In particular, the MFTs of B6 mice (Fig. 2a)

had a larger number of LCs compared with DBA and MRL mice (Fig. 2b and c). The size of these

LCs was also greater in C57BL/6N mice (Fig. 2d) than in other mice strains (Fig. 2e and f). These

observations were confirmed by histoplanimetry (Fig. 2g); the ratios of LC area to total MFT area

were significantly higher in B6 mice than in other mice strains at 3 and 12 months; notably, the

values at 12 months trended higher than the values at 3 months for all examined mice.

In the HE-stained MFT sections, the dark regions of the whole-mount MFT specimens were

observed as clusters of mononuclear cells (Fig 3a–f). We termed these structures MFALCs. All

examined MFALCs differed from the structure of the lymph node, neither surrounded by fibrous

capsules nor formed by lymphatic nodules (Fig. 3d–f). Although MFALCs were observed in all

examined mice, the size and number of MFALCs were more prominent in B6 mice than in DBA and

183   MRL mice. Similar to the light microscope observations of the HE-stained MFT sections, the

184   histoplanimetrical measurements of the ratio of the LC area to the total MFT area (Fig. 3g) revealed

185   a significantly greater ratio in B6 mice than in other mice at 3 and 12 months. In addition, the values

186   at 12 months trended higher than the values at 3 months for all examined mice.

187

188   *Blood vessels and lymphatic vessels in mouse MFALCs*

189   As a characteristic of MFALCs, blood capillaries and venules were observed within the LCs

190   (Fig. 3e and Fig. 4), and several lymphocytes and red blood cells were observed in their lumens.

191   Some endothelial cells in the venules of the MFALCs had abundant cytoplasms and large nuclei,

192   characteristics of HEVs (Fig. 4a and b). Based on the immunohistochemical analysis of PNAd (HEV

193   marker), the endothelial cells of the venules of the MFALCs showed positive reactions, and the

194   positive reactions were stronger in B6 mice (Fig. 4c) than in DBA and MRL mice (Fig. 4d and e) at

195   12 months. No positive reaction in HEV was observed in the serial sections stained with normal IgM

196   controls (Fig. 4f- h).

197   Furthermore, lymphatic vessels positive for LYVE-1 were observed within the MFALCs (Fig.

198   5a-b) as well as the mediastinal fat tissue (Fig. 5c-f), whereas blood vessels containing erythrocytes

199   were not positive for LYVE-1 (Fig. 5c). Interestingly, these lymphatic vessels were abundantly

200   observed in B6 mice (Fig. 5a-c) compared to DBA (Fig. 5d) and MRL mice (Fig. 5e and f) at 12

201   months.

202

203   *Immune cells in mouse MFALCs*

204   To determine the population of immune cells in the MFALCs, immunohistochemical analysis of

205   B220, CD3, CD4, and CD8 was performed to detect B-cells, pan T-cells, Th cells, and Tc cells,

206   respectively. In three strains, B220-positive B-cells and CD3-positive T-cells were observed; the

207   latter was more predominantly observed than the former (Fig. 6a, b, e, and f). For T-cells,

208   CD4-positive Th cells (Fig. 6c and g) were more abundant than CD8-positive Tc cells (Fig. 6d and h).

209   These results were confirmed by histoplanimetry. The immunopositive cell index of CD3 was higher

210   than for other markers in all examined mice, and the index of CD4 was higher than that of CD8 (Fig.

211   6i). No significant strain-specific difference was observed in the populations of MFALC immune

212   cells. Furthermore, few F4/80-positive cells were detected in the MFALC, and no significant

213   strain difference was observed (data not shown).

214   For all examined strains, few CD133-positive cells were observed in the MFALCs (Fig. 7), and

215   these cells were localized within large-sized LCs (Fig. 7a), the lumen of blood vessels (Fig. 7b and

216   c), and small-sized LCs (Fig. 7b and d). The mononuclear cells in the small-sized LCs (Fig. 7b)

217   appeared to be newly aggregated, containing more CD133-positive cells than mononuclear cells in

218   the large-sized LCs (Fig. 7a). No positive cells were observed in the serial sections stained with

219   normal IgG controls (Fig. 7e and f).

220   Immunofluoresence revealed the presence of few c-Kit$^+$/CD127$^+$ cells and many c-Kit$^-$/CD127$^+$

221   cells within the MFALC of C57BL/6 at ** months (Fig. 8a-d). These results were also confirmed by

222   immuhohistochemistry for c-Kit and CD127 (Supplementary figure 1a and b).

223   BrdU-positive cells were observed in the MFALC (Fig. 9). Numerous BrdU-positive cells were

224   observed within the MFALC of B6 mice (Fig. 9c and f) than DBA mice (Fig. 9a and d) at 12 months.

225   Moreover, numerous number of BrdU-positive cells was observed in the MFALC of B6 mice at 12

226   months (Fig. 9c and f) than that at 3 months (Fig. 9b and e).

227

228   **Discussion**

229   *LCs in the MFTs*

230   Adipose tissue is no longer considered an inert tissue that solely functions in energy storage.

231   Other important roles of adipose tissue are emerging, for example, the regulation of various

232   physiological and pathological processes. Recently, there has been much effort to define the roles of

233   adipokine-soluble mediators derived mainly from adipocytes in the interactions between adipose

234   tissues and immunity (MacLaren et al. 2008). Adiponectin and leptin have emerged as the most

235   abundant adipokines produced by adipocytes, thereby redefining adipose tissue as a key component

236   of the endocrine and immune systems (Tilg and Moschen 2006).

237   Novel LCs called FALCs were discovered in the mesenteric adipose tissue of humans and mice

238   (Moro et al. 2010). In the present study, we focused our examination of mouse MFTs at 3 and 12

239   months, corresponding to early and late adulthood, respectively. We discovered LCs in the MFTs of

240   the mouse mediastinum extending from the caval foramen of the diaphragm to the heart. Our

241   histological examinations revealed that these LCs had no fibrous capsules and contained more

242   T-cells than B-cells. Therefore, the structural characteristics and immune cell populations of the

243   MFALCs are similar to the mesenteric FALCs (Moro et al. 2010). Furthermore, the border between

244   the T-cell and B-cell areas was unclear, and no germinal center was observed in the LCs of the

245   mouse MFTs, unlike the milky spot in the omentum (Cranshaw and Leak 1990). The LCs of the

246 MFTs were observed in healthy B6 and DBA mice as well as autoimmune-prone MRL mice. These

247 morphological characteristics and the appearance of MFALCs in healthy mice differed from the

248 tertiary lymphoid follicles and LCs present in the target tissues of various immune diseases, such as

249 synovial tissue in rheumatoid arthritis (Takemura et al. 2001). From these findings, the lymphoid

250 structures that we discovered in the mouse MFTs were clearly distinct from lymphatic nodules and

251 pathological cell infiltrations and were universally observed in different mouse strains. We termed

252 these clusters MFALCs.

253

254 *Age- and strain-specific differences in MFALCs caused by different genetic backgrounds*

255 The putative functions of mouse mesentery FALCs are the self-replication of peritoneal B-cells,

256 the induction of IgA production, and the promotion of an antiparasitic response via Th2 cytokines of

257 Nh cells (Moro et al. 2010; Koyasu et al. 2010; Koyasu and Moro 2011). However, the proper

258 functions of MFALCs in mice and their presence in humans are still unknown. Importantly, in this

259 study, strain- or age-specific changes in MFALCs were observed in mice, and the size of MFALCs

260 increased with age. Age-related changes in immune cells are important for the response to antigen.

261 Briefly, the number of splenic myeloid dendritic cells was higher in middle-aged (8-month-old) and

262 young (3-week-old) B6 mice, and these age-dependent differences in dendritic cells were associated

263 with resistance to *Plasmodium* infection in middle age (Shan et al. 2012). In calves, total mucosal

17

264 leukocytes increased with age in the small intestine; much of this increase was attributed to mucosal

265 CD3+ T-cells. In particular, CD4+ T-cells increased significantly in the jejunum, and CD8+ T-cells

266 increased significantly with age throughout the small intestine (Fries et al. 2011). Furthermore,

267 age-dependent development of the duct-associated lymphoid tissue (DALT) of minor salivary glands

268 was reported in *Macaca fascicularis* (crab-eating macaque); DALT may play a substantial role in the

269 local immunosurveillance of the oral cavity (Nair et al. 1987). These findings suggest the age-related

270 differences in MFALCs might be associated with some immunological functions, relating to

271 increased host responses to pathogens and native antigens.

272 Furthermore, the mouse strain-specific differences were clarified by examination of MFALC

273 morphology. Briefly, the ratio of MFALC area to MFT area was significantly higher in B6 mice than

274 in DBA mice and autoimmune-prone MRL mice. Interestingly, Th1-biased B6 mice are susceptible

275 to hypersensitive pneumonitis, but Th2-biased DBA mice are resistant to it (Butler et al. 2002;

276 Gudmundsson et al. 1998). Hypersensitive pneumonitis is a granulomatous inflammatory lung

277 disease caused by repeated inhalation of organic antigens in humans and mice (Fink 1992; Sharma

278 and Fujimura 1995). Although exposure to pathogenic antigens is widespread in humans, only a

279 minority (5–10%) of the exposed individuals develop clinical disease (Fink 1992), and variations in

280 the susceptibility to hypersensitive pneumonitis, due, for example, to genetic background, might

281 contribute to these differences in humans as well as other animals. Furthermore, eosinophilic

282   macrophage pneumonia is observed more frequently in mice with the B6 genetic background

283   (Murray and Luz 1990; Hoenerhoff et al. 2006). In addition to lung diseases, the genetic background

284   of B6 mice may be associated with aseptic inflammation of the upper urinary tract, which accelerates

285   the pathological effects of the MRL -derived autoimmune susceptibility locus for glomerulonephritis

286   (Ichii et al. 2008; Ichii et al. 2011). Therefore, strain-specific differences in MFALC areas may

287   underlie the differential immune response, mediated by several genetic factors. In particular, the

288   Th1-biased B6 background might be associated with the acceleration of susceptibility to intrapleural

289   disease.

290

291   *Structural characteristics of MFALCs*

292   In the histological examination, we clarified that the majority of the immune cells in the

293   MFALCs were T-cells, rather than B-cells, and specifically CD4-positive Th cells, rather than

294   CD8-positive Tc cells. There were no strain-specific differences in these populations. The mesenteric

295   FALCs also contain CD3-positive T-cells and B220-positive B-cells (Moro et al. 2010). The

296   mesenteric FALCs also contain Th2-type innate lymphocytes called Nh cells (c-Kit$^+$, Sca-1$^+$, IL-2$^+$,

297   IL-2R$^+$, IL-7R$^+$, and IL-33R$^+$) (Moro et al. 2010). Similarly, our results revealed the presence of

298   c-Kit$^+$/CD127$^+$ cells, and we suggested that the MFALCs contained Nh cells. Furthermore, we

299   detected numerous c-Kit-/CD127+cells within the MFALCs. Chiossone et al. 2009 reported that

300   CD127 is also expressed by mouse natural killer cells (NK) lineage cells early during differentiation.

301   Thus, our finding of numerous CD127$^+$ cells within the MFALCs suggest that the MFALCs could be

302   also a source of NK cells.

303   Interestingly, we found blood vessels, such as blood capillaries and venules, in the MFALCs of

304   all examined mice, and the venules showed positive reactions for an HEV marker, PNAd. These

305   PNAd-positive venules were more prominent in B6, which had the largest MFALC area among the

306   examined mouse strains. Lymphocytes are intrinsically mobile; they circulate continuously between

307   the blood and secondary lymphoid tissues. When naive lymphocytes first enter the lymph nodes and

308   Peyer's patches, they adhere to and migrate across the HEV (Kraal and Mebius 1997; Miyasaka and

309   Tanaka 2004). Moreover, LYVE-1-positive lymphatic vessels were observed within the MFALCs

310   and the MFTs. Such lymphatic vessels were more prominent in B6 mice than other examined strains

311   suggesting the major role of lymph vessels for lymphocyte emigration and antigen transport.

312   Furthermore, we found that some CD133-positive cells were observed in the LCs or the lumen

313   of the blood vessels in the MFALCs, indicating the presence of HPCs (Handgretinger and Kuçi

314   2013). It has been suggested that the migration of hematopoietic stem cells occurs through the blood,

315   across the endothelial vasculature, to different organs and to their bone marrow niches via a homing

316   process (Lapidot et al. 2005). From these findings, we propose that immature hematopoietic cells

317   migrate to MFALCs via HEV and act as niches for Th cell production.

318   Our results revealed the presence of BrdU-positive cells within the clusters, indicating that

319   some proliferating cells are present in the MFALCs (Taupin 2007). Our results revealed that

320   numerous BrdU-positive cells were observed in the B6 mice compared to other strains. Moreover,

321   the number of BrdU-positive cells tended to increase with ages. Fulton et al. (2010) showed that

322   regulatory T-cells (Treg) incorporating BrdU rapidly accumulate in the lung-draining mediastinal

323   lymph nodes and lungs following acute respiratory syncytial virus infection. Furthermore,

324   Mannering et al. (2002) revealed that *Listeria* infection causes a dramatic and acute activation and

325   proliferation of T-cells. The present study revealed that normal MFALC structures contain T-cells,

326   B-cells, hematopoietic cells, and proliferating cells in healthy mice. Further studies are required to

327   characterize the immune responses in MFALCs in mice challenged with foreign antigens, focusing

328   especially on the T regulatory response.

329

335

336   **References**

337   Bettelli E, Oukka M, Kuchroo VK (2007) TH-17 cells in the circle of immunity and autoimmunity.

338   Nat Immunol 8: 345-350

339   Butler NS, Monick MM, Yarovinsky TO, Powers LS, Hunninghake GW (2002) Altered IL-4 mRNA

340   stability correlates with Th1 and Th2 bias and susceptibility to hypersensitivity pneumonitis in two

341   inbred strains of mice. J Immunol 169: 3700-3709

342   Charles DM, Kristi K, Jennifer MA, Michelle J (2000) M-1/M-2 macrophages and the Th1/Th2

343   paradigm. J Immunol 164: 6166-6173

344   Chiossone L, Chaix J, Fuseri N, Roth C, Vivier E, Walzer T (2009) Maturation of mouse NK cells is

345   a 4-stage developmental program. Blood 113: 5488–5496.

346   Cranshaw ML, Leak LV (1990) Milky spots of the omentum: a source of peritoneal cells in the

347   normal and stimulated animal. Arch Histol Cytol 53: 165-177

348   Elewa YH, Bareedy MH, Abuel-Atta AA, Ichii O, Otsuka S, Kanazawa T, Lee SH, Hashimoto Y,

349   Kon Y (2010a) Cytoarchitectural differences of myoepithelial cells among goat major salivary

350   glands. Vet Res Commun 34: 557-567

351   Elewa YH, Bareedy MH, Abuel-Atta AA, Ichii O, Otsuka S, Kanazawa T, Lee SH, Hashimoto Y,

352   Kon Y (2010b) Structural characteristics of goat *(Capra hircus)* parotid salivary glands. Jpn J Vet

353   Res 58: 121-135

354   Fink JN (1992) Hypersensitivity pneumonitis. Clin Chest Med 13: 303-309

355   Fiorentino DF, Bond MW, Mosmann TR (1989) Two types of mouse T-helper cell. IV. Th2 clones

356   secrete a factor that inhibits cytokine production by Th1 clones. J Exp Med 170: 2081-2095

357   Fries PN, Popowych YI, Guan LL, Griebel PJ (2011) Age-related changes in the distribution and

358   frequency of myeloid and T cell populations in the small intestine of calves. Cell Immunol 271:

359   428-437

360   Fulton RB, Meyerholz DK, Varga SM (2010) Foxp3$^+$ CD4 regulatory T cells limit pulmonary

361   immunopathology by modulating the CD8 T cell response during respiratory syncytial virus

362   infection. J Immunol 185: 2382-2392

363   Gudmundsson G, Monick MM, Gary W (1998) IL-12 modulates expression of hypersensitivity

364   pneumonitis. J Immunol 161: 991-999

365   Handgretinger R, Kuçi S (2013) CD133-positive hematopoietic stem cells: from biology to medicine.

366   Adv Exp Med Biol 777: 99-111

367   Hoenerhoff MJ, Starost MF, Ward JM (2006) Eosinophilic crystalline pneumonia as a major cause of

368   death in 129S4/SvJae mice. Vet Pathol 43: 682-688

369   Ichii O, Otsuka S, Namiki Y, Hashimoto Y, Kon Y (2011) Molecular pathology of murine ureteritis

370   causing obstructive uropathy with hydronephrosis. PLoS ONE 6: e27783

371   Ichii O, Konno A, Sasaki N, Endoh D, Hashimoto Y, Kon Y (2008) Autoimmune glomerulonephritis

372   induced in congenic mouse strain carrying telomeric region of chromosome 1 derived from

373   MRL/MpJ. Histol Histopathol 23: 411-422

374   Kershaw EE, Flier JS (2004) Adipose tissue as an endocrine organ. J Clin Endocrinol Metab 89:

375   2548-2556

376   Koyasu S, Moro K (2011) Type 2 innate immune responses and the natural helper cell. Immunology

377   132: 475-481

378   Koyasu S, Tanabe M, Takeuchi T, Moro K (2010) Natural helper cells: a new player in the innate

379   immune response against helminth infection. Adv Immunol 108: 21-44

380   Koyasu S, Moro K (2011) Innate Th2-type immune responses and the natural helper cell, a newly

381   identified lymphocyte population. Curr Opin Allergy Clin Immunol 11: 109–114

382   Kraal G, Mebius RE (1997) High endothelial venules: lymphocyte traffic control and controlled

383   traffic. Adv Immunol 65: 347-395

384   Lapidot T, Dar A, Kollet O (2005) How do stem cells find their way home? Blood J 106: 1901-1910

385   Linda DH, Sharon MC, Byungsuk K, Ronald B (2000) Increased severity of pseudomonas

386   aeruginosa corneal infection in strains of mice designated as Th1 versus Th2 responsive. Invest

387   Ophthalmol Vis Sci 41: 805-810

388   MacLaren R, Cui W, Cianflone K (2008) Adipokines and the immune system: an adipocentric view.

389   Adv Exp Med Biol 632: 1-21

390   Mannering SI, Zhong J, Cheers C (2002) T-cell activation, proliferation and apoptosis in primary

391   Listeria monocytogenes infection. Immunology 106: 87-95

392   Mazzucchelli R, Durum SK (2007) Interleukin-7 receptor expression: intelligent design. Nature

393   Reviews Immunology 7:144-154

394   Miyasaka M, Tanaka T (2004) Lymphocyte trafficking across high endothelial venules: dogmas and

395   enigmas. Nat Rev Immunol 4: 360-370

396   Moro K, Yamada T, Tanabe M, Takeuchi T, Ikawa T, Kawamoto H, Furusawa J, Ohtani M, Fujii H,

397   Koyasu S (2010) Innate production of TH2 cytokines by adipose tissue-associated c-Kit$^+$Sca-1$^+$

398   lymphoid cells. Nature 463: 540-544

399   Murray AB, Luz A (1990) Acidophilic macrophage pneumonia in laboratory mice. Vet Pathol 27:

400   274-281

401   Nair PN, Zimmerli I, Schroeder HE (1987) Minor salivary gland duct-associated lymphoid

402   tissue (DALT) in monkeys changes with age. J Dent Res 66: 407-411

403   Nishikawa S, Honda K, Vieira P, Yoshida H (2003) Organogenesis of peripheral lymphoid organs.

404   Immunol Rev 195: 72-80

405   Shan Y, Liu J, Jiang YJ, Shang H, Jiang D, Cao YM (2012) Age-related susceptibility and resistance

406   to nonlethal Plasmodium yoelii infection in C57BL/6 mice. Folia Parasitol (Praha) 59: 153-161

407   Sharma OP, Fujimura N (1995) Hypersensitivity pneumonitis: a noninfectious granulomatosis.

408   Semin Respir Infect 10: 96-106

409   Shimizu S, Sugiyama N, Masutani K, Sadanaga A, Miyazaki Y, Inoue Y, Akahoshi M, Katafuchi R,

410   Hirakata H, Harada M, Hamano S, Nakashima H, Yoshida H (2005) Membranous

411   glomerulonephritis development with Th2-type immune deviations in MRL/lpr mice deficient for

412   IL-27 Receptor (WSX-1). J Immunol 175: 7185-7192

413   Takayama T, Kamadax N, Chinen H et al. (2010) Imbalance of NKp44(+) NKp46(-) and NKp44(-)

414   NKp46(+) natural killer cells in the intestinal mucosa of patients with Crohn's disease.

415   Gastroenterology 139: 882–892

416   Takemura S, Braun A, Crowson C, Kurtin PJ, Cofield RH, O'Fallon WM, Goronzy JJ, Weyand CM

417   (2001) Lymphoid neogenesis in rheumatoid synovitis. J Immunol 167: 1072-1080

418   Taupin P (2007) BrdU immunohistochemistry for studying adult neurogenesis: paradigms, pitfalls,

419   limitations, and validation. Brain Res Rev 53: 198-214

420   Tilg H, Moschen AR (2006) Adipocytokines: mediators linking adipose tissue, inflammation and

421   immunity. Nat Rev Immunol 6: 772-783

422   Zygmunt B, Veldhoen M (2011) T helper cell differentiation more than just cytokines. Adv

423   Immunol 109: 159–196

424

Figure legends

Fig. 1 Gross anatomical localization of mediastinal fat tissue (MFT) in mice: White-colored MFT

(arrows) extending from the diaphragm (D) to the heart (H). DBA/2Cr mouse, 12 months. C: chest

including sternum and ribs. T: thymus

Fig. 2 Mediastinal fat-associated lymphoid clusters in mice. Panels a–f show the stereomicroscopic

photographs of whole-mount hematoxylin-stained mediastinal fat tissues (MFTs) from C57BL/6N

(panels A and D), DBA/2Cr (panels B and E), and MRL/MpJ (panels C and F) mice at 12 months.

The squares in panels a–c indicate the same areas as those in panels d–f. In each panel, the

dark-stained regions represent the lymphoid clusters (LCs) of the MFT (panels d–f, arrows). Larger

numbers and areas of LCs are visible in C57BL/6N mice (panels a and d) compared with DBA/2Cr

(panels b and e) and MRL/MpJ (panels c and f) mice. (g) Percentage of LC area in the total MFT

area in the hematoxylin whole-mount specimens. D and M: Significant differences between

DBA/2Cr (D) and MRL/MpJ (M) mice, analyzed by Tukey's post-hoc test subsequent to ANOVA (p

< 0.05); $n \geq 3$ mice of each strain (at 3 months n = 5, 3, 3 and at 12 months n = 5, 5, 5 in C57BL/6N,

DBA/2Cr, and MRL/MpJ mice, respectively). Values are given as the mean ± SE

Fig. 3 Histological features of mediastinal fat-associated lymphoid clusters in mice. Panels a–f show

443   light microscope photographs of hematoxylin and eosin (HE)-stained mediastinal fat tissue (MFT)

444   sections of C57BL/6N (panels a and d), DBA/2Cr (panels b and e), and MRL/MpJ (panels c and f)

445   mice at 12 months. The squares in panels a–c indicate the same areas as those in panels d–f. In each

446   panel, the accumulation of mononuclear cells is visible in the MFT (panels d–f). More lymphoid

447   clusters (LCs) with larger areas are visible in C57BL/6N mice (panels a and d) compared with

448   DBA/2Cr and MRL/MpJ mice. (g) Percentage of LC area in the total MFT area in the HE-stained

449   sections. D and M: Significant differences between DBA/2Cr (D) and MRL/MpJ (M), analyzed by

450   Tukey's post-hoc test subsequent to ANOVA ($p < 0.05$); n ≥ 3 mice of each strain (at 3 months n = 5,

451   4, 3 and at 12 months n = 4, 4, 4 in C57BL/6N, DBA/2Cr, and MRL/MpJ mice, respectively). Values

452   are given as the mean ± SE

453

454   **Fig. 4** Blood vessels in mediastinal fat-associated lymphoid clusters (MFALCs) in mice. Panels a

455   and b show light microscope photographs of hematoxylin and eosin (HE)-stained mediastinal fat

456   tissue (MFT) sections of C57BL/6N mice at 12 months. Large blood vessels containing lymphocytes

457   (arrowheads) are visible (panel a). In the MFALCs, the endothelial cells of the vessels show

458   epithelioid features with abundant cytoplasms and large nuclei (panels a and b). The squares in panel

459   a indicate the same areas as those in panel b. Panels c–e show light microscope photographs of

460   immunohistochemical stains for the high-abundance endothelial venules marker PNAd in C57BL/6N

461   (panel c), DBA/2Cr (panel d), and MRL/MpJ mice (e) at 12 months. PNAd-positive endothelial cells

462   are visible in the venules of the MFALCs in all of the examined mice (panels c–e, arrows). Panels

463   f–h show the serial section of panels c-e stained by normal rat IgM instead of anti-PNAd antibody,

464   and no normal IgM-positive reaction is observed in the venules.

465

466   **Fig. 5** Lymphatic vessels in mediastinal fat-associated lymphoid clusters in mice. Panels a–f show

467   light microscope photographs of immunohistochemical stains for the lymphatic vessels marker

468   LYVE-1 in C57BL/6N (panels a–c), DBA/2Cr (panel d), and MRL/MpJ mice (e and f) at 12 months.

469   The solid and dotted squares in panel a indicate the same areas as those in panel b and c respectively.

470   LYVE-1-positive lymph vessels are clearly observed in the mediastinal fat tissues (MFTs) (panel b

471   and c, Lv). Erythrocyte-filled blood vessel (panel c, Bv) is negative for LYVE-1. The square in panel

472   e indicate the same area as that in panel f. LYVE-1-positive lymphatic vessels were well developed

473   in the MFTs of C57BL/6N mice (panels a–c) than those of DBA/2Cr mice (panel d) and MRL/MpJ

474   mice (e and f).

475

476   **Fig. 6** Immune cell populations of mediastinal fat-associated lymphoid clusters (MFALCs) in mice.

477   Panels a–h show light microscope photographs of immunohistochemical stains for B220 (B-cells,

478   panels a and e), CD3 (pan T-cells, panels b and f), CD4 (helper T-cells, panels c and g), and CD8

479   (cytotoxic T-cells, panels d and h) in C57BL/6N mice at 12 months. The squares in panels a–d

480   indicate the same areas as those in panels e–h. Cells immunopositive for each antigen are visible in

481   the MFALC of C57BL/6N mice. (i) Index of immune cell populations in the MFALCs of the mice. a,

482   b, c, and d: Significant differences between B220 (a), CD3 (b), CD4 (c), and CD8 (d) in same mouse

483   strain, m: Significant difference with MRL/MpJ in same antigen, analyzed by Tukey's post-hoc test

484   subsequent to ANOVA ($p < 0.05$); n = 3 mice in each strain. Values are given as the mean ± SE

485

486   **Fig. 7** CD133-positive cells of mediastinal fat-associated lymphoid clusters (MFALCs) in mice.

487   Panels a–d show light microscope photographs of immunohistochemical stains for CD133 (marker

488   for hematopoietic progenitor cells)-positive cells in C57BL/6N mice at 12 months. The dotted and

489   solid squares in panel b indicate the same areas as those in panel c and d respectively. Few positive

490   cells are visible in the MFALC (panel a, arrows) and in the lumen of the MFALC vessels (v) (panel b

491   and c). In panel d, the smaller-sized lymphoid clusters showed numerous CD133-positive cells.

492   Panels e and f are stained by normal rabbit IgG instead of anti-CD133 antibody for negative control,

493   and the square in panel e indicate the same area as those in panel f. No normal IgG-positive cells

494   were observed in the MFALC (Panels 7e and f).

495

496   Fig. 8 c-Kit- and CD127-positive cells of mediastinal fat-associated lymphoid clusters (MFALCs) in

497 mice. Panels are representative images of immunofluoresce for c-Kit (panel a, green) and CD127

498 (panel b, red) with nuclear staining by Hoechst (panel c, blue) in C57BL/6 at ** months. Merged

499 image is shown in panel d, demonstrating the presence of few c-Kit+/ CD127+ cells (arrows) and

500 many c-Kit-/ CD127+ cells within the MFALC.

501

502 Fig. 9 Proliferating cells in the mediastinal fat-associated lymphoid clusters (MFALCs) in mice.

503 Proliferating cells were detected by immunohistochemistry for BrdU in DBA/2Cr at 12 months

504 (panel a) and C57BL/6N mice at 3 and 12 months (panels b and c respectively). Panels d, e and f are

505 higher magnification to the square area in panels a, b and c respectively. Note fewer BrdU-positive

506 cells are visible within the MFALCs in DBA/2Cr mice (panel a and d) compared to C57BL/6N mice

507 (panels b and e) at 12 months. Interestingly, in C57BL/6N mice, BrdU-positive cells are abundantly

508 observed at 12 months (panels b and e) compared to 3 months (panels c and f).

Figure 1.
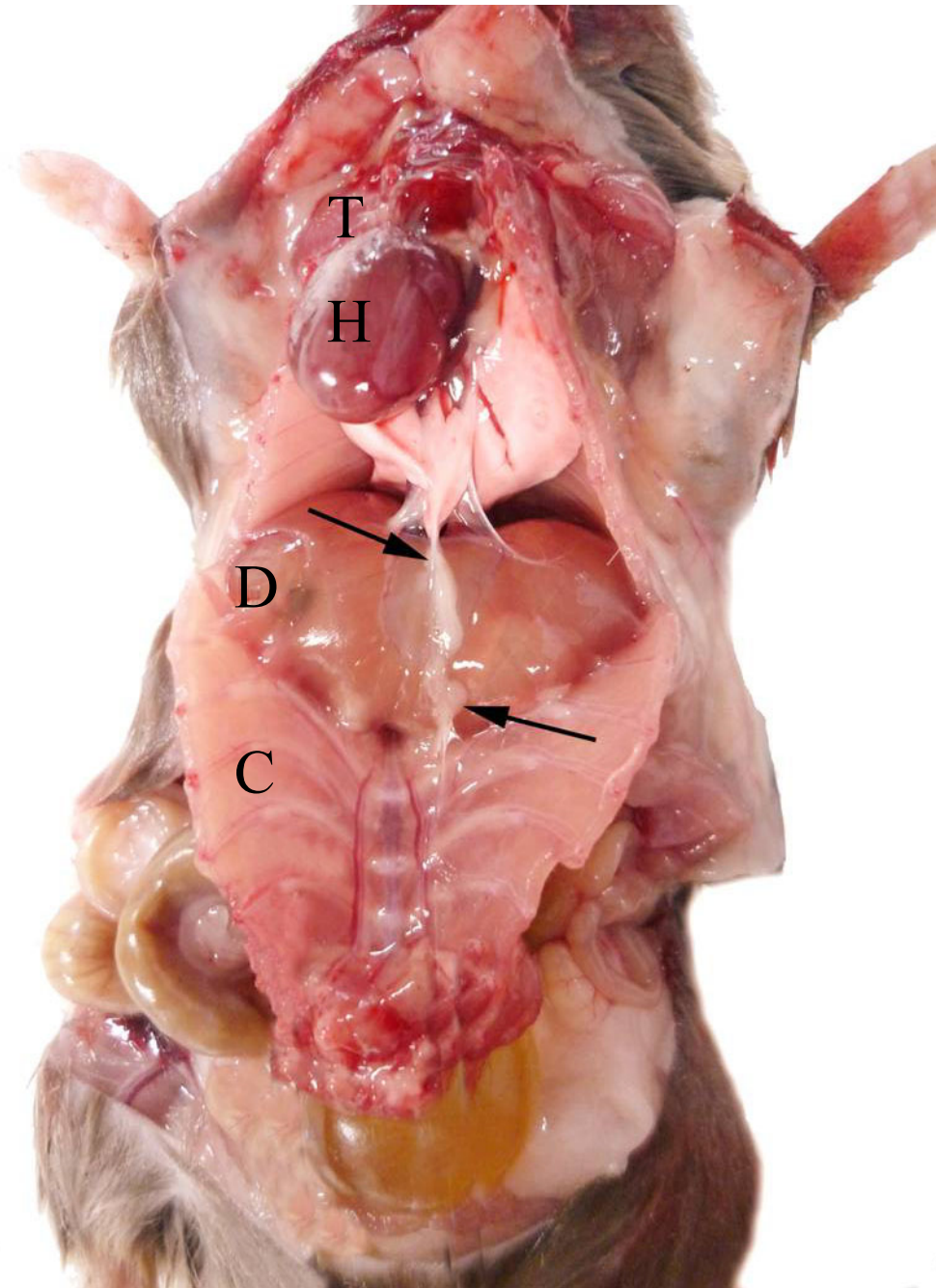
Figure 2.
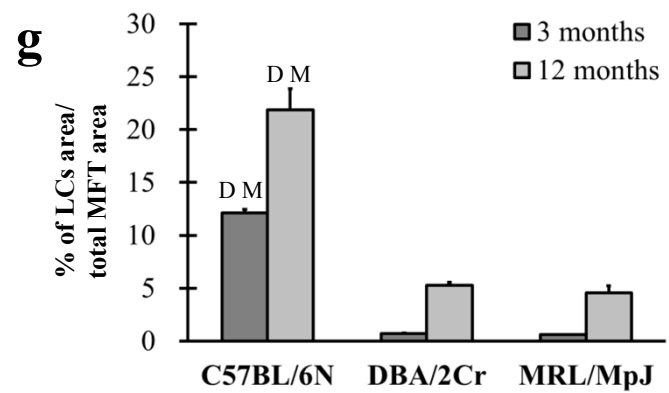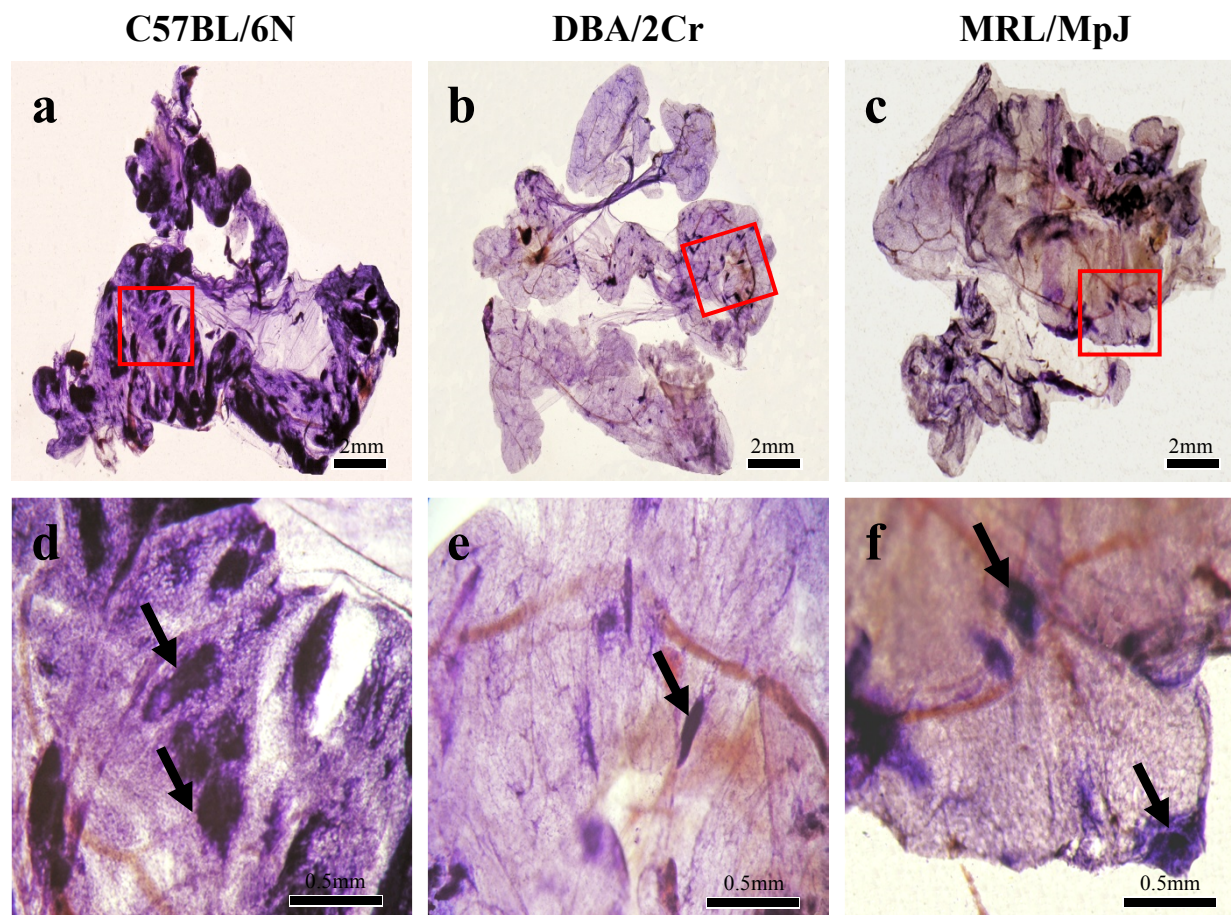
Figure 3.
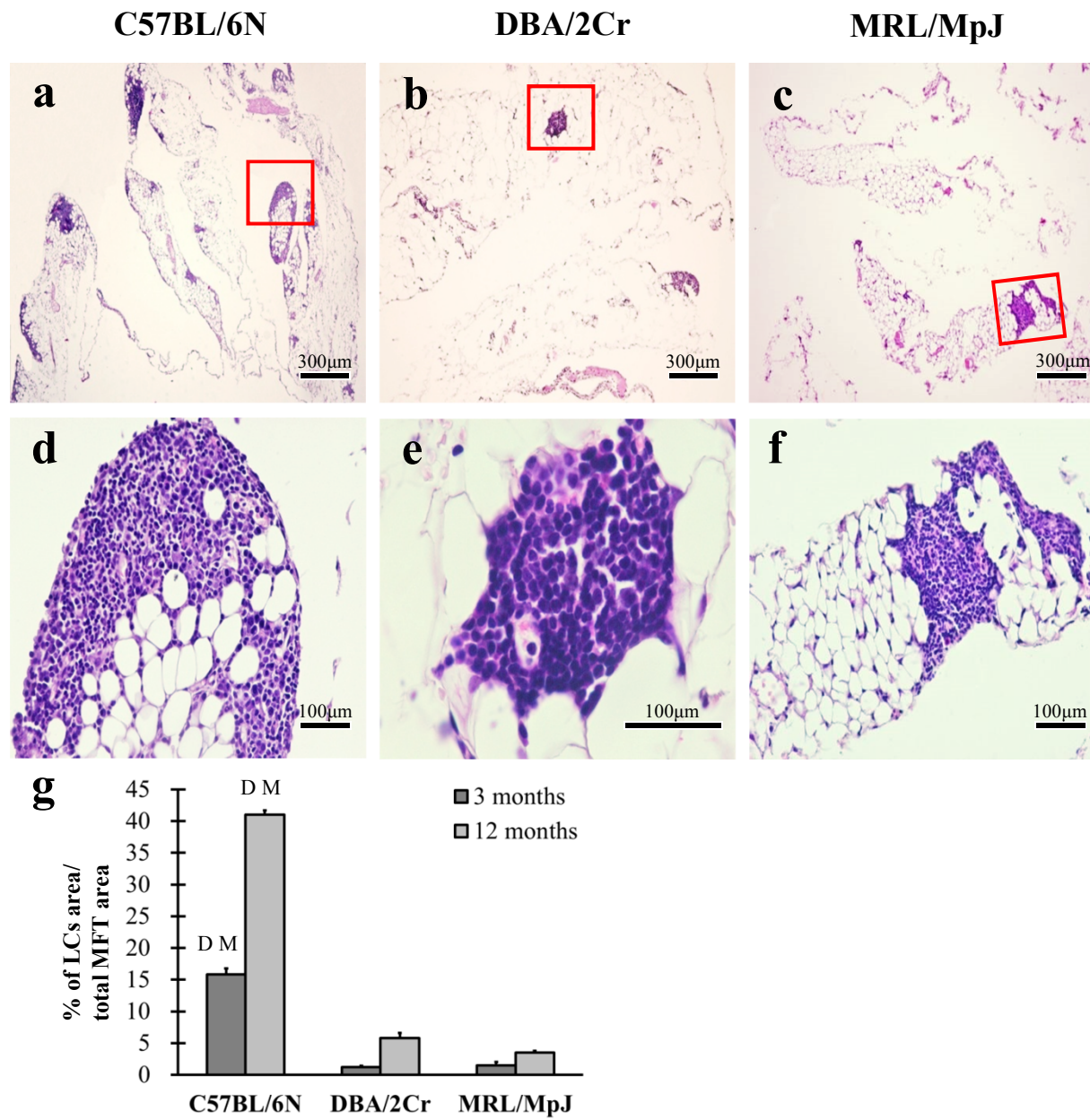
Figure 4.
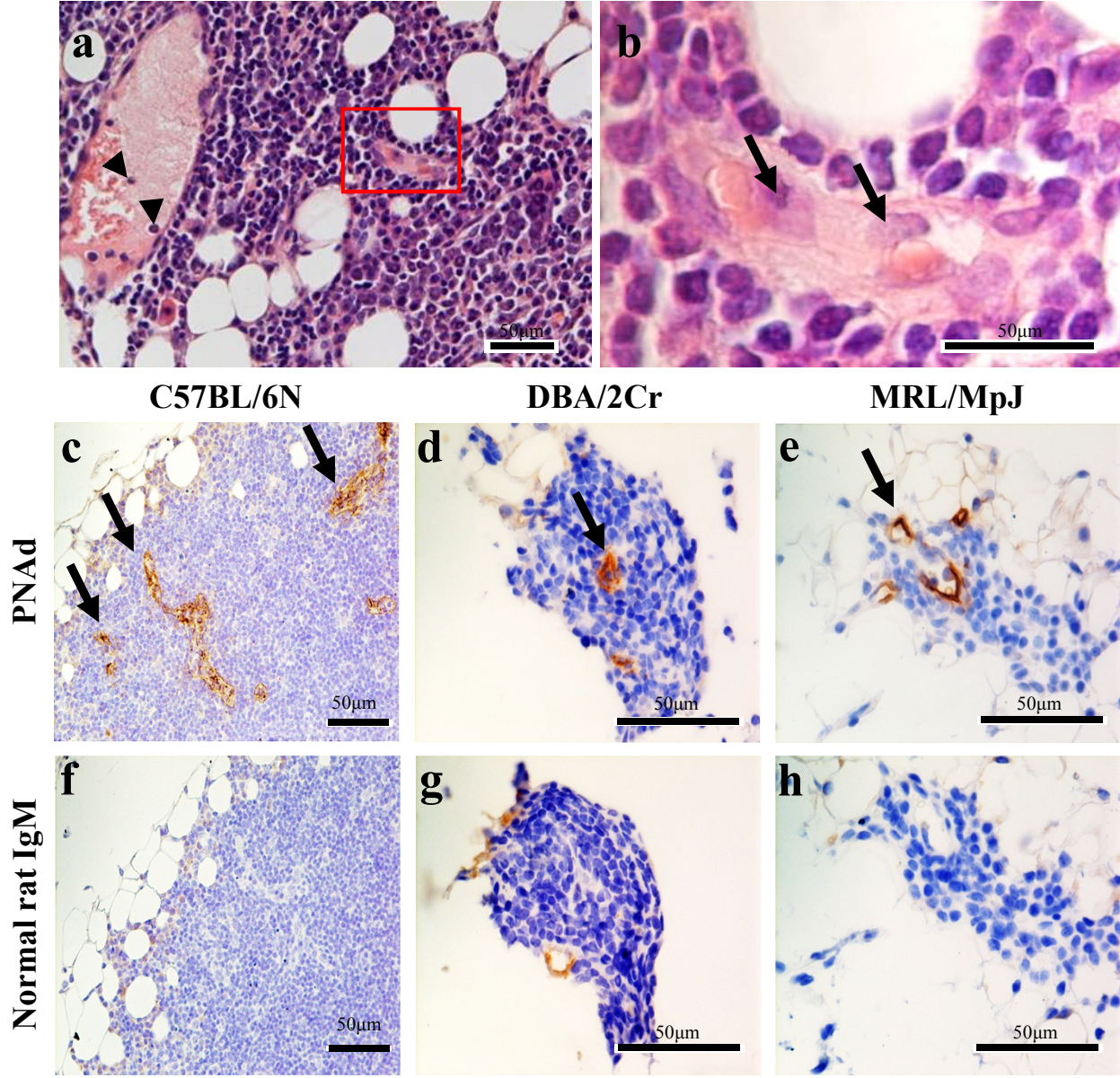
Figure 5.
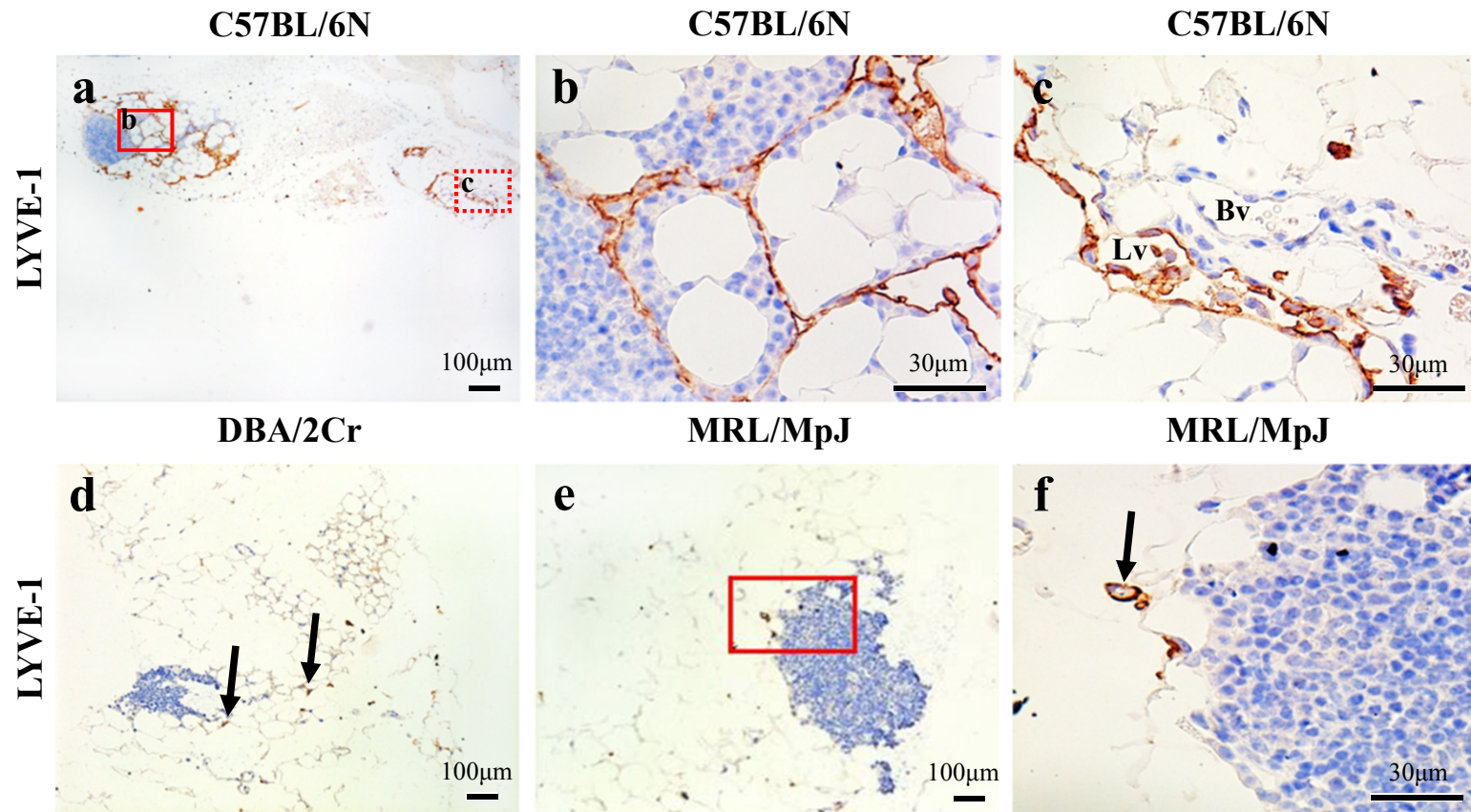
Figure 6.
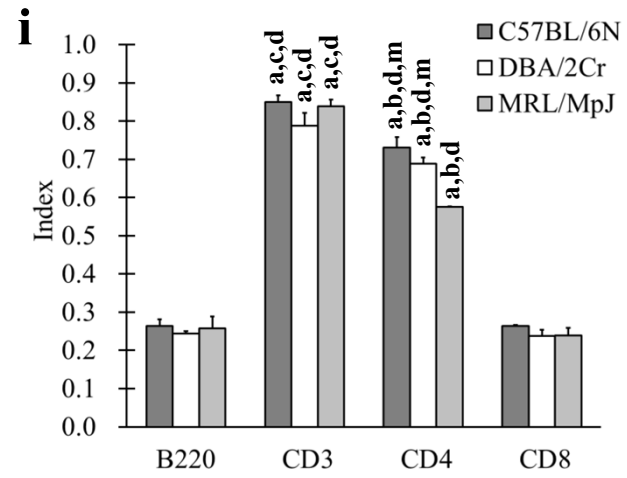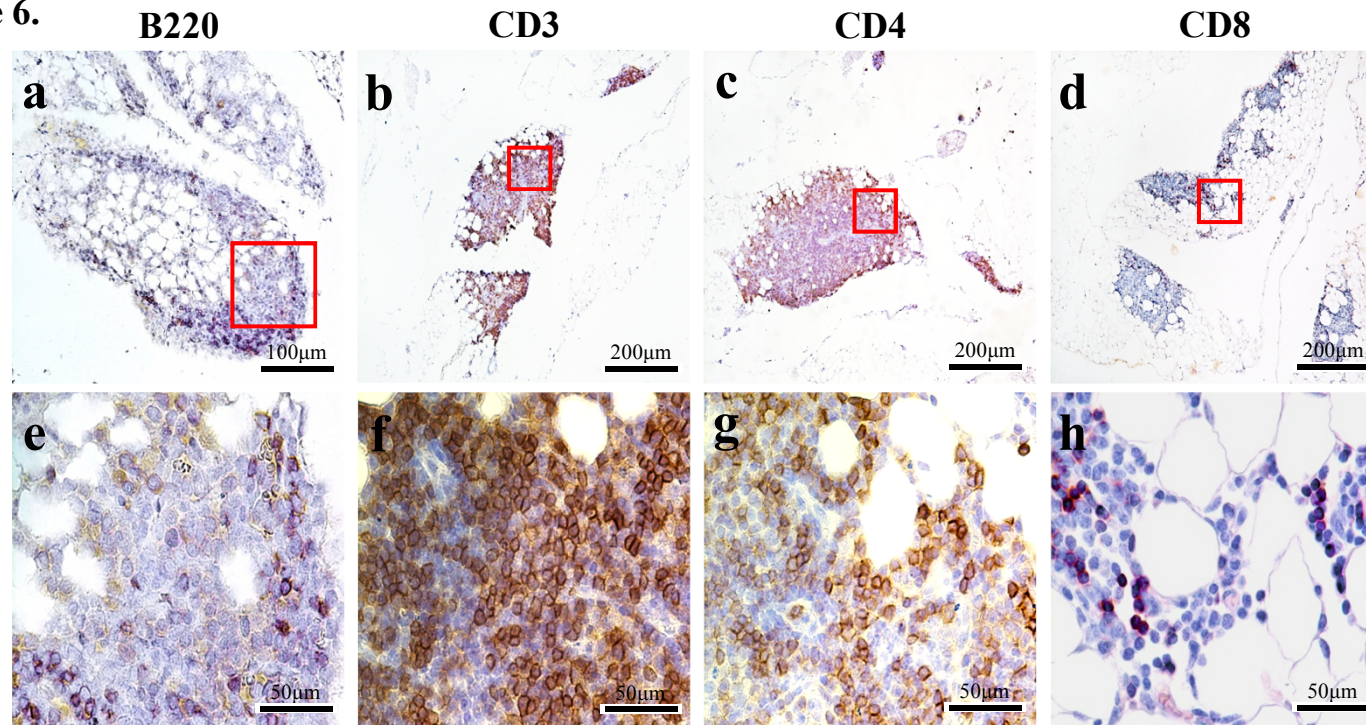
Figure 7.

Figure 8.

Figure 9.